photonics

MDPI

Article

Luminescence and Gamma Spectroscopy of Phosphate Glass Doped with Nd^{3+}/Yb^{3+} and Their Multifunctional Applications

Bilel Charfi [1], Kamel Damak [1], Mohammed S. Alqahtani [2,3], Khalid I. Hussein [2,4], Ali M. Alshehri [5], Nehal Elkhoshkhany [6,7], Abdullah L. Assiri [2], Khaled F. Alshehri [2], Manuela Reben [8] and El Sayed Yousef [5,9,*]

1 LaMaCoP, Faculty of Sciences of Sfax, University of Sfax, Sfax 3018, Tunisia; bilel.charfi@ipeis.usf.tn (B.C.); kamel.damak@ipeis.usf.tn (K.D.)
2 Department of Radiological Sciences, College of Applied Medical Sciences, King Khalid University, Abha 61421, Saudi Arabia; mosalqhtani@kku.edu.sa (M.S.A.); kirahim@kku.edu.sa (K.I.H.); 438801913@kku.edu.sa (A.L.A.); 438801909@kku.edu.sa (K.F.A.)
3 BioImaging Unit, Space Research Centre, Department of Physics and Astronomy, University of Leicester, Leicester LE1 7RH, UK
4 Department of Medical Physics and Instrumentation, National Cancer Institute, University of Gezira, Wad Medani 2667, Sudan
5 Physics Department, Faculty of Science, King Khalid University, Abha 61413, Saudi Arabia; amshehri@kku.edu.sa
6 Physics Department, College of Arts and Sciences Jouf University, Tabrjal 74713, Saudi Arabia; nmak2002@hotmail.com
7 Department of Material Science, Institute of Graduate Studies and Researches, Alexandria University, 163 Horreya Avenue, Shatby, Alexandria 21526, Egypt
8 Faculty of Materials Science and Ceramics, AGH—University of Science and Technology, Al. Mickiewicza 30, 30-059 Cracow, Poland; manuelar@agh.edu.pl
9 Research Center for Advanced Materials Science (RCAMS), King Khalid University, Abha 61413, Saudi Arabia
* Correspondence: ayousf@kku.edu.sa

check for updates

Citation: Charfi, B.; Damak, K.; Alqahtani, M.S.; Hussein, K.I.; Alshehri, A.M.; Elkhoshkhany, N.; Assiri, A.L.; Alshehri, K.F.; Reben, M.; Yousef, E.S. Luminescence and Gamma Spectroscopy of Phosphate Glass Doped with Nd^{3+}/Yb^{3+} and Their Multifunctional Applications. *Photonics* **2022**, *9*, 406. https://doi.org/10.3390/photonics9060406

Received: 8 April 2022
Accepted: 3 June 2022
Published: 8 June 2022

Publisher's Note: MDPI stays neutral with regard to jurisdictional claims in published maps and institutional affiliations.

Abstract: A new glass with a composition of $40P_2O_5$-30ZnO-20LiCl-$10BaF_2$ (in mol%), doped with $3.5Nd_2O_3$-$3.5Yb_2O_3$, was fabricated by the quenching melt technique. The luminescence (PL) and gamma spectroscopy of the glass were investigated systematically. The spectroscopic parameters of the prepared glass, such as the optical energy gap, Judd–Ofelt parameters Ω_k (where k = 2, 4 and 6), lifetimes and branching ratio of the Nd^{3+}/Yb^{3+} level, were evaluated. Moreover, the shielding parameters, such as the linear and mass attenuation coefficients, mean free path and half-value layer, were evaluated. The prepared glass had a spectroscopic quality factor (Ω_4/Ω_6) of 0.84, which is about three-times larger than that of the most standard laser host, Nd^{3+}:YAG. The energy of the 2P1/2 (Nd^{3+}) level (~23,250 cm^{-1}) was twice the energy of the Yb^{3+} transition (~10,290 cm^{-1}). The value of the emission cross section ($\sigma_{em}(\lambda)$) of Nd^{3+}:$^4F_{3/2} \rightarrow {}^4I_{9/2}$ and Yb^{3+}:$^2F_{5/2} \rightarrow {}^2F_{7/2}$ were 2.23×10^{-24} cm^2 and 2.88×10^{-24} cm^2, respectively. The fabricated glass had a high emission cross section and low mean free path parameters, which makes the fabricated glass a potential candidate for multifunctional applications, such as laser emissions for medical purposes.

Keywords: phosphate glass; Nd^{3+}/Yb^{3+} ions; optical spectroscopy; Judd–Ofelt analysis; luminescence; shielding

1. Introduction

The codoped ions Nd^{3+} and Yb^{3+} are some of the best examined rare-earth elements and are used in fiber lasers. In both glasses and crystals, efficient energy transfer between Nd^{3+} and Yb^{3+} ions has been established. Nd^{3+}/Yb^{3+} glasses are applied as compact sources in non-linear microscope technology in image processing with a THz frequency [1,2].

It is worth exploring the higher excited states of Nd^{3+} involved in the energy transfer from Nd^{3+} to Yb^{3+}. The lanthanide ion Yb^{3+} emits a wavelength of approximately 1000 nm, which may be absorbed without losing any energy. Moreover, the longer lifetime and broader absorption and emission bands of Yb^{3+} ions allow greater energy-storage efficiency in comparison with other rare earth ions, namely the Nd^{3+} ions [3,4]. Although the lanthanide ion Yb^{3+} has just one excited state, around 10,000 cm^{-1} above the ground state, the pump wavelength range of Yb^{3+} ions is limited to 980 nm by this simple energy level scheme. Down-conversion may occur if a suitable sensitizer with energy levels of 20,000 cm^{-1}, two times the energy of Yb^{3+}, is used [5].

However, laser glasses have been specifically designed for photodynamic therapy surgery and medical radiation technology. Researchers investigated the optical and shielding properties of such glasses for their usefulness as a safety replacement device in medical workplaces, such as X-ray and atomic projects in the field of inventions, V-ray equipment, gamma camera rooms and examination workplaces for computed tomography (CT) [6,7]. The radiation protecting characteristics of Erbium Zinc–Tellurite glass were inspected to compare a vast range of radiation energies for health and medical imaging applications (20, 30, 40 and 60 keV) [8]. Furthermore, the laser diodes for fiber optical intercommunicating applications exhibit near-infrared (NIR) discharge at a wavelength of 1.54 µm that can be employed in armed forces, detective work and medical investigations facilities [9].

Therefore, we fabricated phosphate laser glass with the composition P_2O_5-ZnO-LiCl-BaF_2 (PZLB) as the host lattice due to the low matrix phonon energy codoped with Nd^{3+}/Yb^{3+} ions, which decreases the non-radiative transition rate to lower states. This is beneficial for the cross-relaxation energy transfer between Nd^{3+} and Yb^{3+}. Thus, the spectroscopic properties of this glass were comprehensively investigated; furthermore, the energy transfer efficiency from Nd^{3+} to Yb^{3+} is also discussed. In addition to that, we measured attenuation radiation parameters, such as the linear attenuation coefficient, LAC; the mass attenuation coefficient, MAC; half-value layer, HVL; and the mean free path, MFP, of the prepared glass.

2. Materials and Methods

A homogeneity Nd^{3+}/Yb^{3+}doped glass with the composition (in mol%) $40P_2O_5$-30ZnO -20LiCl-10BaF_2-3.5Nd_2O_3-3.5Yb_2O_3, referred to as PZLBNdYb glass, was prepared by the melt quenching technique. We mixed the chemical very well in an alumina crucible. We placed it into a muffle furnace to be melted at 1200 °C for 1 h following the melt quenching technique. The molten chemical mixture was then quenched in a preheated copper mold. The quenched glass was heat-treated at 450 °C for 2 h at the beginning of the annealing process to eliminate any strain on sample molecules.

The density of the glass was measured using a gas pycnometer (Model: UltraPyc 1200e). The measured density of the PZLBNdYb glass sample was $\rho = 4.426 \pm 0.001$ g/cm^3. Using a UV-VIS-NIR spectrophotometer, the optical absorption spectra of the glasses were measured in the wavelength range of 190–2500 nm (JASCO, V-570).

The concentration of Nd^{3+} (or Yb^{3+}) ions can be calculated by the following expression:

$$N_{Nd^{3+}} = 2\frac{3.5\rho A_v}{100M} \quad (1)$$

where M is the molecular weight of PZLBNdYb glass and A_v is Avogadro's number. The concentration of the dopant Nd^{3+} or Yb^{3+} in PZLBNdYb glass was $N_{Nd^{3+}} = N_{Yb^{3+}} = 1.405 \times 10^{27}$ ions/m^3.

The shielding parameters—the linear attenuation coefficient (LAC), mass attenuation coefficient (MAC), half-value layer (HVL) and mean free path (MFP)—of the proposed sample were measured using the NaI detector system (SPECTECH-NaI 1.5 PX 1.5/2.0 IV, S/N 010723-6) connected to a computer-based multichannel analyzer (MCA). Different gamma sources (Am^{241}-5µCI-59.5 keV, Cs^{137}-5µCI-662 keV, Co^{60}-5µCI-1170 and 1330 keV) were used to produce a collimated beam at the detector level. Our group study, in Ref. [10], de-

tailed the experimental setup utilized for detecting the incident and transmission radiation intensities in Figure 1.

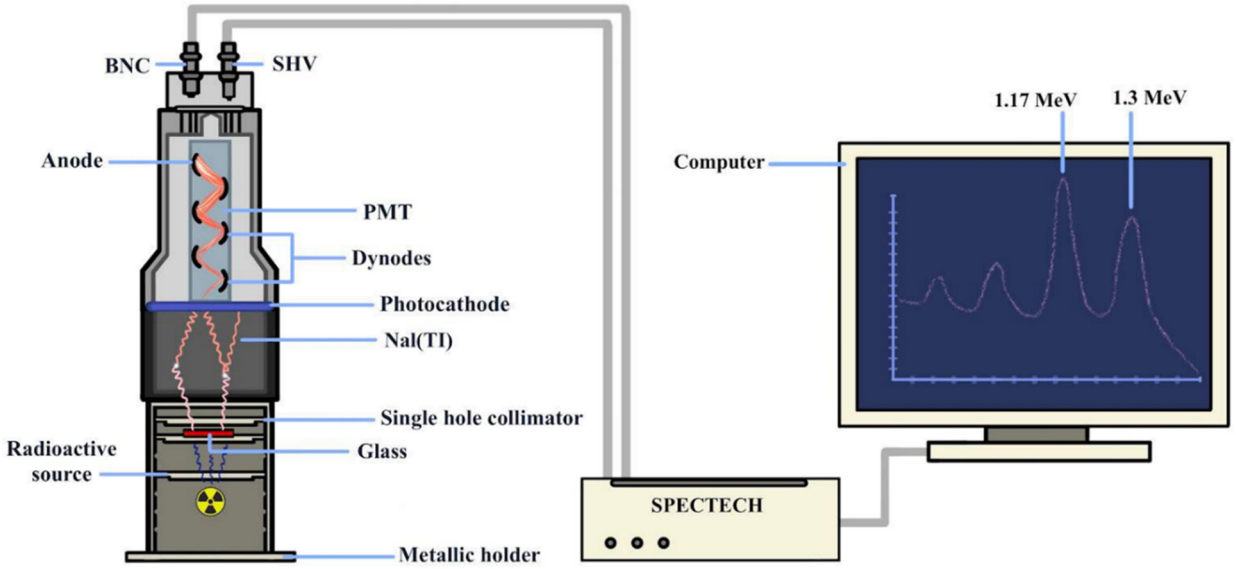

Figure 1. The experimental setup used for measuring the shielding parameters for the proposed sample [10].

The values of μ_m, μ, HVL and MFP parameters can be calculated using the following relations.

$$\begin{cases} \mu = \frac{ln\frac{I_0}{I}}{x}, \\ \mu_m = \frac{ln\frac{I_0}{I}}{\rho x}, \\ HVL = \frac{0.693}{\mu}, \\ \text{and } MFP = \frac{1}{\mu} \end{cases} \quad (2)$$

In Ref. [10], we detailed the experimental setup utilized for detecting the incident and transmission radiation intensities in Figure 1.

3. Results and Discussion

Absorption Spectroscopy, Optical Energy Gap and Judd–Ofelt Analysis

The UV–Vis–NIR absorption spectra for the PZLBNdYb sample are recorded in Figure 2. The absorption spectra displayed seven bands centered around 352, 428, 470, 522, 580, 628, 682, 744, 802, 882 and 980 nm. All bands originated from the absorption transition from the ground state ($^4I_{9/2}$) to different excited states of the Nd^{3+}($^4f_3$) ion, except the 980 nm peak, which corresponds to the $^2F_{7/2} \rightarrow {}^2F_{5/2}$ absorption transition for ytterbium ions.

The Nd^{3+} ion bands detected are comparable to those previously described [11,12], except for minor changes in the peak positions and relative intensities. This can be attributed to the nature of various ligand fields of different glass matrixes [13]. The maximum absorption coefficient is observed at 590 nm wavelength, corresponding to the $^4I_{9/2} \rightarrow {}^2G_{7/2}$ + $^4G_{5/2}$ hypersensitive transition. In contrast, the absorption peak of $^4I_{9/2} \rightarrow {}^2H_{11/2}$ (at 628 nm) was the lowest and was weak enough to be considered in the computation.

The Stark structure was poorly resolved for all bands due to the inhomogeneous broadening, and nearby energy levels overlapped—appearing as a single peak in the measured spectra. The number of long orders in the host causes changes in the micro symmetry surrounding the Nd^{3+} ions, resulting in amplification of the absorption bands. In other words, the linewidth of the various transitions is a measure of the Stark splitting of the J-manifold. The inhomogeneous broadening is due to the site-to-site variation in the local field seen by the rare earth ion.

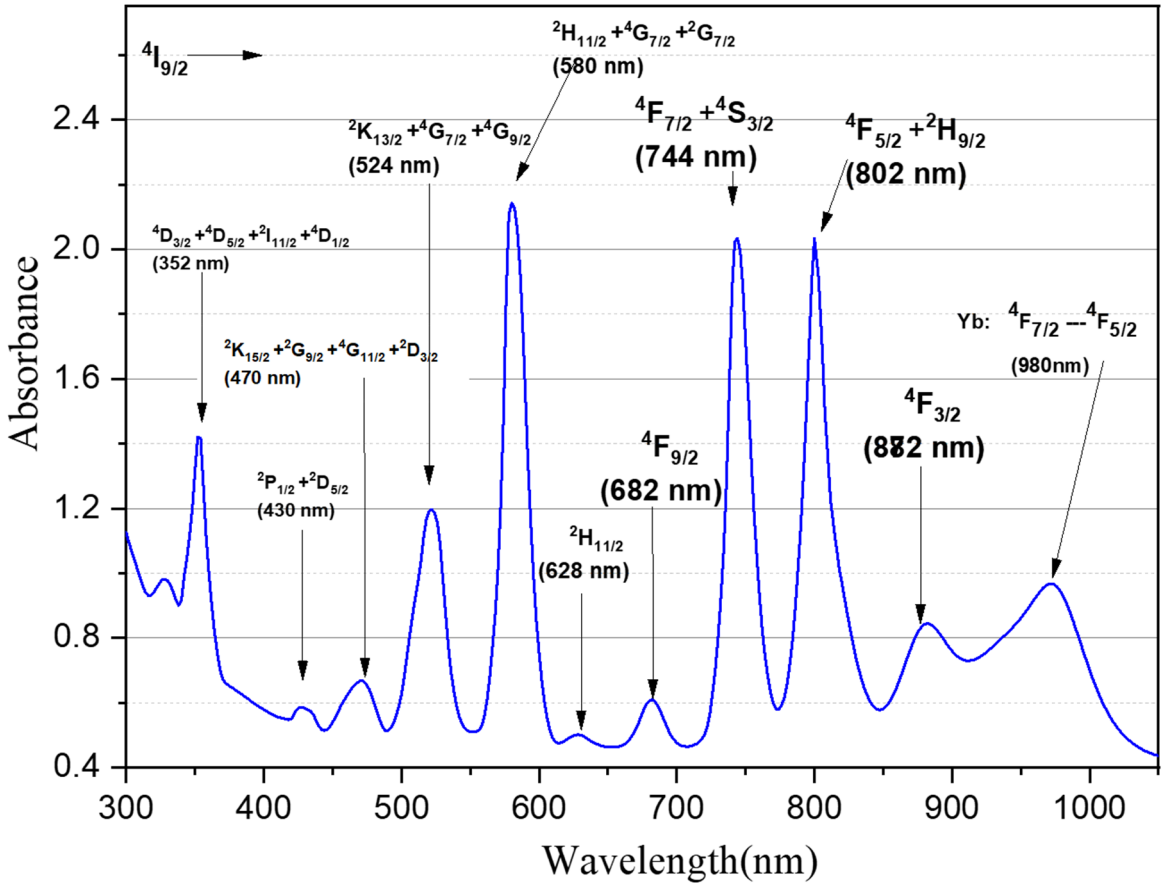

Figure 2. Absorption spectra of PZLBNdYb glass. The upper transition state is identified for each peak.

Extrapolation of the linear relation, Equation (3), of the plotted absorption curves yielded the optical energy gap, E_{opt}, which reflected the transition from localized states at the top of the valence band into localized ones in the conduction band or vice versa.

The optical energy gap, E_{opt}, was calculated by using the absorption spectra of the produced glass as follows [7];

$$[\alpha(\nu)h\nu]^{\frac{1}{r}} = A(h\nu - E_{opt}) \quad (3)$$

where $\alpha(\nu)$ is the absorption coefficient, A is a constant, $h\nu$ is the incident radiation's photon energy, and r is an index that varies depending on the transition type (direct or indirect). The best fit to the result obtaining that $r = 2$ indicated the indirect allowed transition in the gap. The optical band edge is obtained by extrapolating from the linear range in plots of $(\alpha h\nu)^{\frac{1}{2}}$ versus $h\nu$, as shown in Figure 3. The optical energy gap E_{opt} was 4.41 eV higher than phosphate glasses doped with rare earth [11–17]. This wide optical energy gap range shows that this glass is superior and a good medium as an acceptor of the rare earth donor from the optical fiber (non-linear/laser waveguide).

To determine the spectroscopic parameters of this glass system, the Judd–Ofelt (JO) analysis was applied to the absorption intensities of Nd^{3+} doped in PZLBNdYb. The detailed applications of the JO model can be found in the literature [17,18]. A brief outline of the JO analysis is given hereafter.

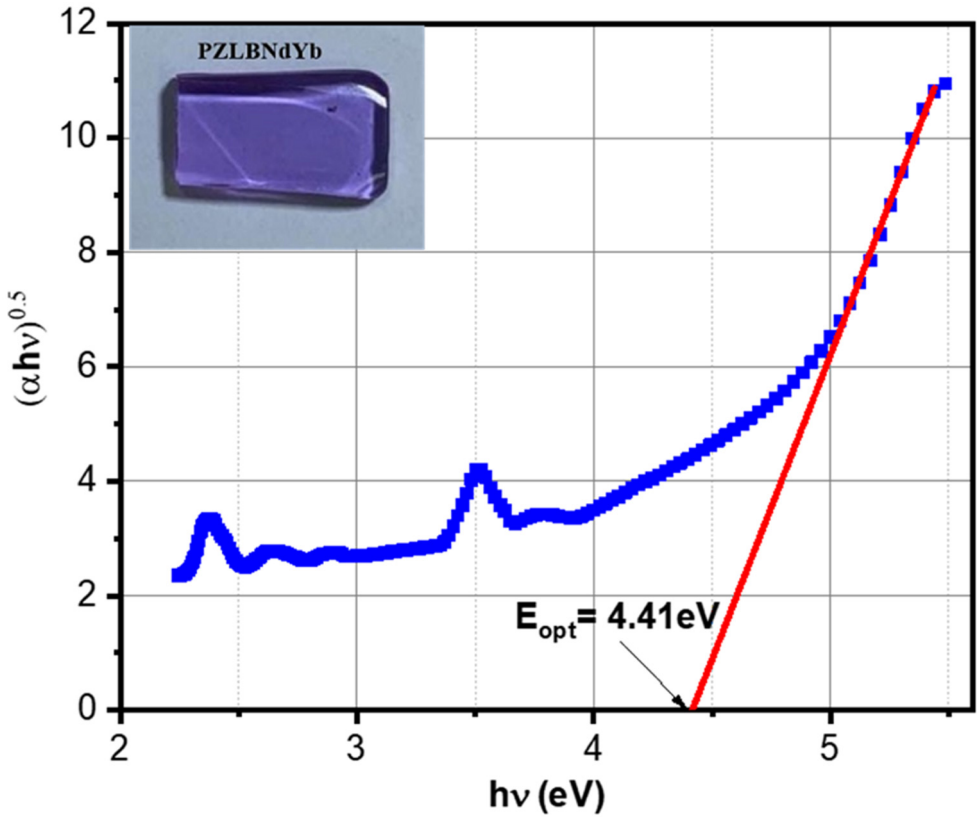

Figure 3. Relation between ($\alpha h\nu$) and ($h\nu$) of the prepared glass PZLBNdYb.

The measured line strength $S_{\exp}(J \to J')$ of a given band is determined by the following expression:

$$S_{\exp}(J \to J') = \frac{9n}{(n^2+2)^2} \cdot 4\pi\varepsilon_0 \cdot \frac{3c \cdot h \cdot (2J+1)}{8\pi^3 e^2} \cdot \frac{2.303}{N \cdot l \cdot \lambda} \cdot \Gamma(\lambda) \quad (4)$$

where c is the velocity of light, h is the Planck's constant, e is the elementary charge, J is the angular momentum of the initial state, N is the density of Nd^{3+} ions, λ is the mean wavelength of the absorption bands, l is the thickness of the studied sample (l = 7.82 mm), and n is the refractive index dispersion. $\Gamma = \int OD(\lambda) \cdot d\lambda$ is the total area under the absorbed band and can be used to calculate the experimental integrated optical density in the wavelength range.

The magnetic-dipole contribution has been ignored in this work as its impact on the measured line strength is relatively negligible for absorption transitions of Nd^{3+} ion [15,19,20].

The results of the intensity measurements and line strength calculations for transitions of Nd^{3+} ions are reported in Table 1.

On the other hand, in the Judd–Ofelt theory, the line strength $S_{cal}(J \to J')$ between initial state J characterized by (S, L, J) and the final state J' given by (S', L', J') can be calculated by the following expression [17,18]:

$$S_{cal}(J \to J') = \sum_{t=2,\,4,\,6} \Omega_t \left| \left\langle SLJ \| U^{(t)} \| S'L'J' \right\rangle \right|^2 \quad (5)$$

where Ω_t (t = 2, 4, 6) denote the Judd–Ofelt variables and $\| U^{(t)} \|^2$ (t = 2, 4, 6) are the doubly reduced matrix elements.

The reduced matrix elements could be found in the literature [13,21–23]. For two or more manifolds, the reduced matrix elements are taken as the sum of the correspond-

ing matrix elements. The values of matrix elements for each absorption band are given in Table 1.

Table 1. The results of the intensity measurements and line strength calculations for absorption transitions of Nd^{3+} doped in PZLBNdYb glass, $\delta_{rms} = 1.019 \times 10^{-25}$ m^2.

Transitions: $^4I_{9/2}\rightarrow$	λ (nm)	ν (cm^{-1})	$\|\|U^2\|\|^2$	$\|\|U^4\|\|^2$	$\|\|U^6\|\|^2$	Γ ($nm \cdot cm^{-1}$)	S_{exp} (10^{-26} m^2)	S_{cal} (10^{-26} m^2)
$^4D_{3/2} + {}^4D_{5/2} + {}^2I_{11/2} + {}^4D_{1/2}$	352	28,409	0.0050	0.5256	0.0478	7.8511	24.489	22.244
$^2P_{1/2} + {}^2D_{5/2}$	430	23,255	0.0000	0.0369	0.0021	0.5117	1.2993	1.4960
$^2K_{15/2} + {}^2G_{9/2} + {}^2D_{3/2} + {}^4G_{11/2}$	470	21,276	0.0010	0.0472	0.0364	3.1505	7.3169	3.4488
$^2K_{13/2} + {}^4G_{7/2} + {}^4G_{9/2}$	524	19,083	0.0665	0.2182	0.1271	16.22	34.053	15.772
$^4G_{5/2} + {}^2G_{7/2} + {}^2H_{11/2}$	580	17,241	0.9737	0.5968	0.0777	27.298	51.294	52.438
$^4F_{9/2}$	682	14,662	0.0009	0.0092	0.0417	2.6065	4.1785	2.2393
$^4F_{7/2} + {}^4S_{3/2}$	744	13,440	0.0010	0.045	0.6598	25.624	37.600	31.252
$^4F_{5/2} + {}^2H_{9/2}$	802	12,468	0.0102	0.2451	0.5127	14.853	20.269	32.523
$^4F_{3/2}$	882	11,467	0.0000	0.2293	0.0548	2.0965	2.6098	11.164

Based on Equations (4) and (5), a fitting between experimental and calculated line strengths of the absorption transitions provides the values of the three JO parameters. A least squares fitting of S_{exp} to S_{cal} values was used to compute the Ω_t (t = 2, 4, 6) parameters for the studied PZLBNdYb sample.

According to matrix element and S_{exp} values, one can notice that, principally, the Ω_2 parameter depends on $^4I_{9/2}\rightarrow{}^4G_{5/2} + {}^2G_{7/2} + {}^2H_{11/2}$ (580 nm) and $^4I_{9/2}\rightarrow{}^4D_{3/2} + {}^4D_{5/2} + {}^2I_{11/2} + {}^4D_{1/2}$ (352 nm) peak intensities, Ω_4 also depends on this later peak, while Ω_6 depends on the $^4I_{9/2}\rightarrow{}^4F_{7/2} + {}^4S_{3/2}$ (744 nm) absorbance. Thus, one can consider that the $^4I_{9/2}\rightarrow{}^4D_{3/2} + {}^4D_{5/2} + {}^2I_{11/2} + {}^4D_{1/2}$ (352 nm) transition is the most influencing line in the Ω_t computation for Nd^{3+} doped glasses.

The obtained JO parameters of Nd^{3+} in PZLBNdYb glass are given in Table 2 with those for Nd^{3+} doped in other hosts. For Yb^{3+}, it is not possible to determine the three Ω_t intensity parameters because only one transition (corresponding to the $^2F_{7/2}\rightarrow{}^2F_{5/2}$ transition at 980 nm) can be observed.

Table 2. Comparison of Judd–Ofelt parameters (Ω_t, $\times 10^{-20}$ cm^2) of PZLBPr glass along with other systems.

Systems	Ω_2	Ω_4	Ω_6	Trend	χ
PZLBNdYb [Present Work]:	0.269	0.379	0.447	$\Omega_2 < \Omega_4 < \Omega_6$	0.84
LGBaBNd05 [12]	6.10	6.85	9.83	$\Omega_2 < \Omega_4 < \Omega_6$	0.69
YAG:Nd^{3+} [24]	0.20	2.70	5.00	$\Omega_2 < \Omega_4 < \Omega_6$	0.54
LHG-750 [25]	4.60	4.80	5.60	$\Omega_2 < \Omega_4 < \Omega_6$	0.85
PKFBAN10 [26]	4.92	3.67	5.26	$\Omega_4 < \Omega_2 < \Omega_6$	0.70
ZnBBi [27]	3.56	4.30	4.87	$\Omega_2 < \Omega_4 < \Omega_6$	0.88
Nd^{3+}:fluorotellurite(n = cst) [11]	4.21	5.97	5.45	$\Omega_2 < \Omega_6 < \Omega_4$	1.09
Nd^{3+}:fluorotellurite($n \neq$ cst) [11]	4.51	6.34	6.16	$\Omega_2 < \Omega_6 < \Omega_4$	1.02
Nd^{3+} doped Y_2O_3 ceramic [22]	8.84	9.82	4.44	$\Omega_6 < \Omega_2 < \Omega_4$	2.21
75$NaPO_3$-24CaF_2-1NdF_3 [28]	2.78	4.16	5.56	$\Omega_2 < \Omega_4 < \Omega_6$	0.74
3000 ppm Nd^{3+}/Yb^{3+} in phosphate [13]	1.897	0.820	1.834	$\Omega_4 < \Omega_6 < \Omega_2$	0.44
30,000 ppm Nd^{3+}/Yb^{3+} in phosphate [13]	0.2339	0.6437	0.9598	$\Omega_2 < \Omega_4 < \Omega_6$	0.67
NCB:Nd glasses [14]	1.50	0.93	2.39	$\Omega_4 < \Omega_2 < \Omega_6$	0.39
PMZ1.5 Nd [15]	4.69	4.72	2.98	$\Omega_6 < \Omega_2 < \Omega_4$	1.58
AEBTNd0.1 [16]	3.694	2.865	2.548	$\Omega_2 < \Omega_4 < \Omega_6$	1.12
P_2O_5-Li_2O_3-GdF_3-Nd_2O_3 [29]	8.55	11.54	10.25	$\Omega_2 < \Omega_6 < \Omega_4$	1.13
Nd^{3+} doped zinc phosphate [30]	4.67	5.53	5.77	$\Omega_2 < \Omega_4 < \Omega_6$	0.95

The calculated Judd–Ofelt parameters are in good agreement with literature values for Nd^{3+} doped glasses. The JO intensity parameters for this PZLBNdYb glass followed the trend $\Omega_6 > \Omega_4 > \Omega_2$. This trend is similar to that of commercial laser glasses [25], YAG:Nd^{3+} [24], as

well as LGBaBNd [12], 30,000 ppm Nd^{3+}/Yb^{3+} phosphate [13], AEBTNd0.1 [16], ZnBBi [27], $75NaPO_3$-$24CaF_2$-$1NdF_3$ [28] glasses (see Table 2).

The intensity parameter, Ω_2, strongly correlated with the local structure of the rare earth ions and the covalency degree lanthanide–O bonds, which is equivalent to the dynamic polarization of the ligands. In comparison, the Ω_4 and Ω_6 parameters depend upon the rigidity and viscosity of the host glasses [16,31,32]. Similar to the other reported work (mentioned in Table 2), the larger Ω_6 in the present glass indicates its high rigidity, and the lower Ω_2 indicates the higher asymmetry and lower covalency between the Nd-O group in this PZLBNdYb glass.

The obtained Ωt values are used to recalculate the transition line strengths Scal of the absorption bands from Equation (5) and deduce the rms deviation. The root-mean-square (rms) deviation of the fit between experimental and calculated oscillator strengths is deduced by the expression. $\delta_{rms} = (\sum (S_{\exp} - S_{cal})^2/(N_{trans} - 3))^{1/2}$

The value of the rms deviation calculated in the present work is equal 1.019×10^{-25} m^2. This slightly elevated value of rms deviation can be explained by overlaps of absorption bands in the UV region.

The spectroscopic quality factor, $\chi = \Omega_4/\Omega_6$, is an important characteristic in predicting the stimulated emission cross section for the laser active media. In the case of Nd^{3+}, it is indicated that the smaller the ratio, the more intense the laser $^4F_{3/2} \rightarrow {}^4I_{11/2}$ transition. Due to the decreased matrix element's zero value, this occurs $\left\langle {}^4F_{3/2} \| U^{(t)} \| {}^2I_J \right\rangle$ of Nd^{3+} ion [33–35].

For this PZLBNdYb glass, the spectroscopic quality factor (Ω_4/Ω_6) was 0.84, which is about three-times larger than that of the standard laser host Nd^{3+}:YAG. Usually, χ is in the range from 0.22 to 1.5 for Nd^{3+} in several host materials (see Table 2).

According to the absorption spectrum of Figure 2, the emission band $^4F_{3/2} \rightarrow {}^4I_{9/2}$ of Nd^{3+} partially overlapped with the absorption band $^2F_{5/2} \rightarrow {}^2F_{7/2}$ of Yb^{3+}, which ensures that the Yb^{3+} ion absorbs the NIR light very effectively. The wideness and lowness of the Yb^{3+} absorption peak ascribe to the $Nd^{3+} \rightarrow Yb^{3+}$ energy transfer. However, the short separation distance between ions, estimated as $d = (3/4\pi N)^{1/3} = 7$Å, confirms an efficient $Nd^{3+} \rightarrow Yb^{3+}$ energy transfer.

It is worth noting that systems based on Nd^{3+}/Yb^{3+} energy transfers are interesting because they combine the Yb^{3+} ion's good laser emission characteristics with the Nd^{3+} ion's multiple intense absorption bands, which could be used for pumping with a variety of sources (laser diodes, flash lamps, solar radiation, etc.).

The $^4F_{3/2}$ level for Nd^{3+} ions is the only exciting J manifold that did not relax predominantly by a multiphonon process. This level fluoresces in the four bands ascribed to $^4F_{3/2} \rightarrow {}^4I_{9/2}$ at 882 nm, $^4F_{3/2} \rightarrow {}^4I_{11/2}$ around 1056 nm, $^4F_{3/2} \rightarrow {}^4I_{13/2}$ at 1318 nm and $^4F_{3/2} \rightarrow {}^4I_{15/2}$ at 1870 nm. The emission line strengths attributed to the transition from $^4F_{3/2}$ to ^4I_J manifolds were computed through Equation (5) using the Ω_2, Ω_4 and Ω_6 parameters. The $Nd^{3+} \rightarrow Yb^{3+}$ energy transfer competes with the self-quenching of Nd^{3+} emission due to the cross-relaxation of the resonant process ($^4F_{3/2} + {}^4I_{9/2} \rightarrow {}^4I_{15/2} + {}^4I_{15/2}$) or phonon-assisted process ($^4F_{3/2} + {}^4I_{9/2} \rightarrow {}^4I_{15/2} + {}^4I_{13/2}$) between the Nd^{3+} ions.

The spontaneous emission probability $A_{JJ'}$ for a transition from a J-multiplet to a lower J'-multiples is calculated as:

$$A_{J \rightarrow J'} = \frac{1}{4\pi\varepsilon_0} \frac{64\pi^4 e^2 v^3 n(n^2+2)^2}{27h(2J+1)} S_{cal} \quad (6)$$

S_{cal} is the corresponding emission line strength.

The radiative lifetime τ for electric dipole transitions between an excited state (J) and the lower-lying terminal manifolds (J') could also be estimated as follows:

$$\tau = \frac{1}{\sum_{J'} A_{J \to J'}} \quad (7)$$

The sum is taken over all final states J'. The fluorescence branching ratio is a critical parameter to the laser designer; it might be calculated by predicting the relative strength of lines from certain excited states and describing the possibility of achieving stimulated emission from a specific transition. It is determined by:

$$\beta = A_{J \to J'}.\tau \quad (8)$$

Table 3 shows the radiative transition probabilities ($A_{J \to J'}$), radiative lifetimes (τ) and branching ratios (β) of energy levels $^4I_{9/2}$,$^4I_{11/2}$, $^4I_{13/2}$, $^4I_{15/2}$ and $^4F_{3/2}$ of Nd^{3+} ion in the PZLBNdYb glass.

Table 3. Spectroscopic parameters of the PZLBNdYb glass system.

Transition	Energy (cm^{-1})	A (s^{-1})	T (ms)	B (%)
$^4F_{3/2} \to {}^4I_{9/2}$	882	253.24	1.644	41.639
$^4F_{3/2} \to {}^4I_{11/2}$	1051	294.29		48.389
$^4F_{3/2} \to {}^4I_{13/2}$	1329	57.675		9.4834
$^4F_{3/2} \to {}^4I_{15/2}$	1827	2.9709		0.4884
$^4I_{15/2} \to {}^4I_{9/2}$	1626	1.6995	118.78	20.187
$^4I_{15/2} \to {}^4I_{11/2}$	2478	4.5382		53.905
$^4I_{15/2} \to {}^4I_{13/2}$	4878	2.1812		25.909
$^4I_{13/2} \to {}^4I_{9/2}$	2440	5.935	126.42	75.028
$^4I_{13/2} \to {}^4I_{11/2}$	5040	1.9754		24.972
$^4I_{11/2} \to {}^4I_{9/2}$	4730	2.5817	387.34	100

A critical factor in the success of the Nd^{3+} amplifier is the long lifetime of the $^4F_{3/2}$ metastable state that permits the required high population inversion to be obtained. The radiative lifetime of the $^4F_{3/2}$ state was calculated to be 1.644 ms, which is an essential metric to consider when considering the pumping need for the laser action threshold. The trend of lifetimes appears to be decreasing as $^4I_{11/2} > {}^4I_{13/2} > {}^4I_{15/2} > {}^4F_{3/2}$. The branching ratios for emission transitions are steadily decreasing as follows: $^4I_{13/2} \to {}^4I_{9/2} > {}^4I_{15/2} \to {}^4I_{11/2} > {}^4F_{3/2} \to {}^4I_{11/2} > {}^4F_{3/2} \to {}^4I_{9/2} > {}^4F_{3/2} \to {}^4I_{13/2} > {}^4F_{3/2} \to {}^4I_{15/2}$. A similar tendency of branching ratios was noticed by Zamen et al. [12] and James et al. [14].

In order to understand the probability of lasing action between $^4F_{3/2} \to {}^4I_{11/2}$ and $^4F_{3/2} \to {}^4I_{9/2}$ of Nd^{3+} ion, the essential parameters, such as the peak wavelength (λ), transition probability (A) and branching ratio (β) for the $^4F_{3/2} \to {}^4I_{11/2}$ and $^4F_{3/2} \to {}^4I_{9/2}$ transitions of different Nd^{3+}-doped glasses are collected in Table 4.

The branching ratios of $^4F_{3/2} \to {}^4I_{9/2}$ and $^4F_{3/2} \to {}^4I_{11/2}$ transition in the PZLBNdYb glass was ~41% and 48%, respectively, which is comparable to BSKNLNd10 and PNbKA [36,37], PZLNNd1.0 [38], phosphate [14] and Nd^{3+}-doped P_2O_5-Li_2O_3-GdF_3 [29] glasses (see Table 4).

The proposed glasses have suitable spectroscopic quality factors, radiative lifetime and branching ratio values for lasing materials in the infrared region. In both glasses and crystals, efficient energy transfer between Nd^{3+} and Yb^{3+} ions has been established. The Nd^{3+} energy diagram, presented in Figure 4, shows the grouping of levels. The gap between gathering levels guarantees a large radiative probability of transition among both groups. By contrast, the small energy gap between the levels inside each group favors the multiphonon relaxation process.

Table 4. Peak position (λ, nm), radiative transition probabilities (A, s^{-1}), calculated branching ratios (β) and radiative lifetime (τ, ms) for $^4F_{3/2}\rightarrow{}^4I_{9/2}$ and $^4F_{3/2}\rightarrow{}^4I_{11/2}$ transitions of Nd^{3+}-doped phosphate glasses.

Host	Transition	Wavelength (nm)	A (s^{-1})	T (ms)	B (%)
PZLBNdYb [PW]	$^4F_{3/2}\rightarrow{}^4I_{9/2}$ $^4F_{3/2}\rightarrow{}^4I_{11/2}$	882 1051	253.24 294.29	1.644	41 48
P_2O_5-Li_2O_3-GdF_3-Nd_2O_3 [29]	$^4F_{3/2}\rightarrow{}^4I_{9/2}$ $^4F_{3/2}\rightarrow{}^4I_{11/2}$	874 1065	2917 3091	0.151	44 47
PZLNNd1.0 [38]	$^4F_{3/2}\rightarrow{}^4I_{9/2}$ $^4F_{3/2}\rightarrow{}^4I_{11/2}$	873 1052	398 342		41 53
3000 ppm Nd^{3+}/Yb^{3+} in phosphate glasses [14]	$^4F_{3/2}\rightarrow{}^4I_{9/2}$ $^4F_{3/2}\rightarrow{}^4I_{11/2}$	896 1056	403.8 716.2	0.77	31 55
30,000 ppm Nd^{3+}/Yb^{3+} in phosphate glasses [13]	$^4F_{3/2}\rightarrow{}^4I_{9/2}$ $^4F_{3/2}\rightarrow{}^4I_{11/2}$	896 1056	280.2 395.1	0.13	36 51

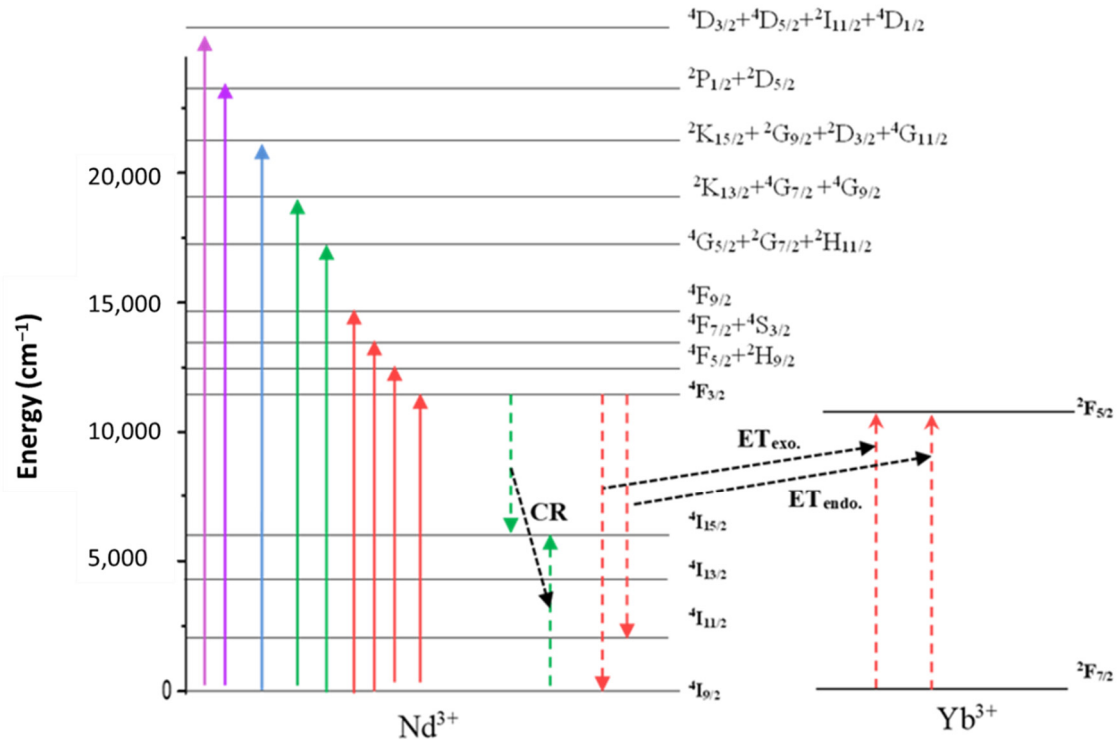

Figure 4. Energy level diagrams of Nd^{3+} and Yb^{3+} ions.

According to Figure 4, the energy of the $^4F_{3/2}$ emitting level of Nd^{3+} is located slightly higher than the $^2F_{5/2}$ emitting level of Yb^{3+}; thus, an $Nd^{3+}\rightarrow Yb^{3+}$ energy transfer could take place via a phonon-assisted process ($^4F_{3/2}$, $^2F_{7/2}\rightarrow{}^4I_{9/2}$, $^2F_{5/2}$ exothermic nonresonant transfer) and ($^4F_{3/2}$, $^2F_{7/2}\rightarrow{}^4I_{11/2}$, $^2F_{5/2}$ endothermic nonresonant transfer). Furthermore, it was suggested that only a negligible resonant $Yb^{3+}\rightarrow Nd^{3+}$ back transfer occurred. However, the phonon-assisted energy transfer from Nd^{3+} to Yb^{3+} as the way of quantum cutting is noticed. The energy of the $^2P_{1/2}(Nd^{3+})$ level (~23,250 cm^{-1}) was approximately twice the energy of the Yb^{3+} transition (~10,290 cm^{-1}) and the phonon-assisted energy transfer can be described as follows: Nd^{3+} emission: $^2P_{1/2}(Nd^{3+})\rightarrow{}^4I_{9/2}(Nd^{3+})$; Yb^{3+} absorption: $2\ {}^2F_{7/2}\ (Yb^{3+})\rightarrow 2\ {}^2F_{5/2}(Yb^{3+})$.

Normally, the $^2F_{7/2}$ and $^2F_{5/2}$ Stark levels of Yb^{3+} ions split into several sublevels due to the crystal field effect [36]. Here, the absorption spectrum was fitted by Lorentz fitting, shown in Figure 5.

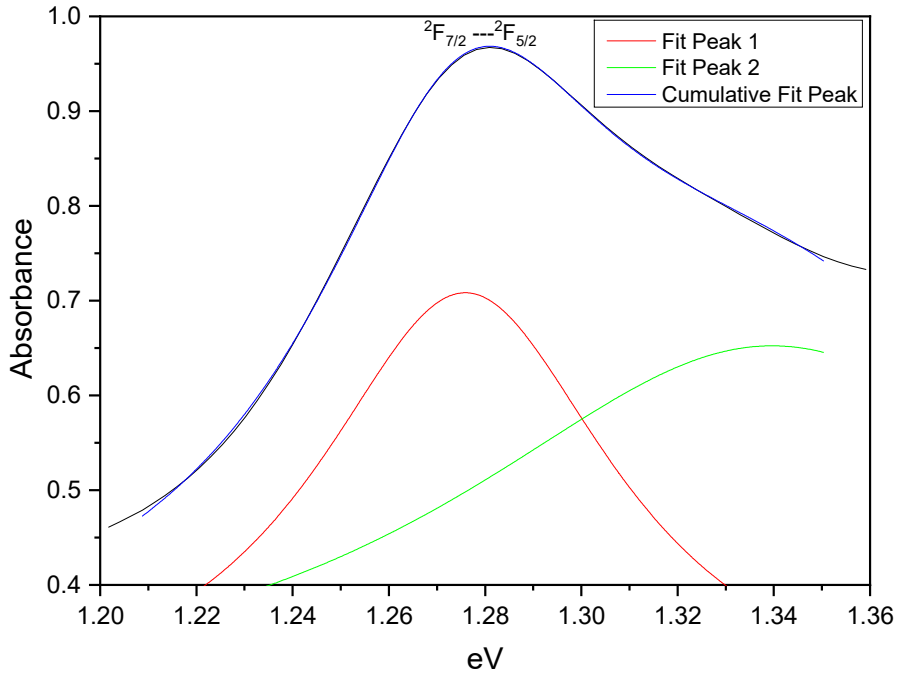

Figure 5. Deconvolution of the Yb^{3+} absorption peak.

From Figure 5, the spectrum fits two absorption bands attributed to transitions between the ground state of $^2F_{7/2}$ and two Stark-splitting levels of $^2F_{5/2}$. In principle, I_{974}/I_{928} 3; however, in our case, this ratio is reduced to ~1.5, which is related to the $Nd^{3+} \rightarrow Yb^{3+}$ energy transfer.

The absorption and emission cross sections must be calculated to determine the lasing performance. The absorption cross section of a transition may be calculated as:

$$\sigma_{abs}(\lambda) = \frac{2.303}{Nl} \times D(\lambda) \quad (9)$$

where $D(\lambda)$ is the optical density, l is the thickness of the sample, and N is the ion concentration in the sample. Furthermore, the emission cross section, $\sigma_{em}(\lambda)$, of Nd^{3+}: $^4F_{3/2} \rightarrow {}^4I_{9/2}$ and Yb^{3+}:$^2F_{5/2} \rightarrow {}^2F_{7/2}$ can be calculated from the absorption cross section by:

$$\sigma_{em}(\lambda) = \sigma_{abs}(\lambda) \cdot \frac{Z_l}{Z_u} \cdot exp\left[hc \cdot (kT)^{-1} \cdot \left[(\lambda_{ZL})^{-1} - (\lambda)^{-1}\right]\right] \quad (10)$$

where the lower and upper levels of the optical transition are Z_l and Z_u. T is the temperature, k is the Boltzmann constant, and Z_{ZL} is the wavelength at which the lower Stark sublevels of emitting multiplets and receiving multiplets intersect at this transition (zero-phonon line). However, at high temperatures, the partition function ratios of the lower and higher states Z_l/Z_u simply degenerate into a weighting of the two states. The precise Z_l/Z_u glass value is not known. The zero-phonon line was considered to be 882 nm for Nd^{3+} and 972 nm for Yb^{3+} in the following calculation, which assumes a Z_l/Z_u ratio of 10/4 for Nd^{3+} and 8/6 for Yb^{3+}.

Figure 6 shows the Absorption and emission cross section of prepared glass PZLB-NdYb. The computed $\sigma_{Yb\ abs}$ at (λ_p = 980 nm) of Yb^{3+}:$^2F_{5/2} \rightarrow {}^2F_{7/2}$ was 2.01 × 10^{-24} cm^2, and that of Nd^{3+} for $^4I_{9/2} \rightarrow {}^4F_{3/2}$ at $\sigma_{Nd\ abs}$(λ_p = 882 nm) was 1.71 × 10^{-24} cm^2. The $\sigma_{Yb\ abs}$ was larger than that of Nd^{3+} $\sigma_{Nd\ abs}$ in the NIR region, confirming that the $Nd^{3+} \rightarrow Yb^{3+}$ dominates the $Nd^{3+} \rightarrow Nd^{3+}$ energy transfer. Since the absorption cross section of Yb^{3+} is larger than that of Nd^{3+} at equal densities, it can be considered that Yb^{3+} acts as an acceptor, while Nd^{3+} is the donor in this NIR region. The values of $\sigma_{em}(\lambda)$ of Nd^{3+}: $^4F_{3/2} \rightarrow {}^4I_{9/2}$ and Yb^{3+}:$^2F_{5/2} \rightarrow {}^2F_{7/2}$ are equal to 2.23 × 10^{-24} cm^2 and 2.88 × 10^{-24} cm^2, respectively. The

larger cross sections of the emission transitions indicate that the intense NIR emitting can be conditioned.

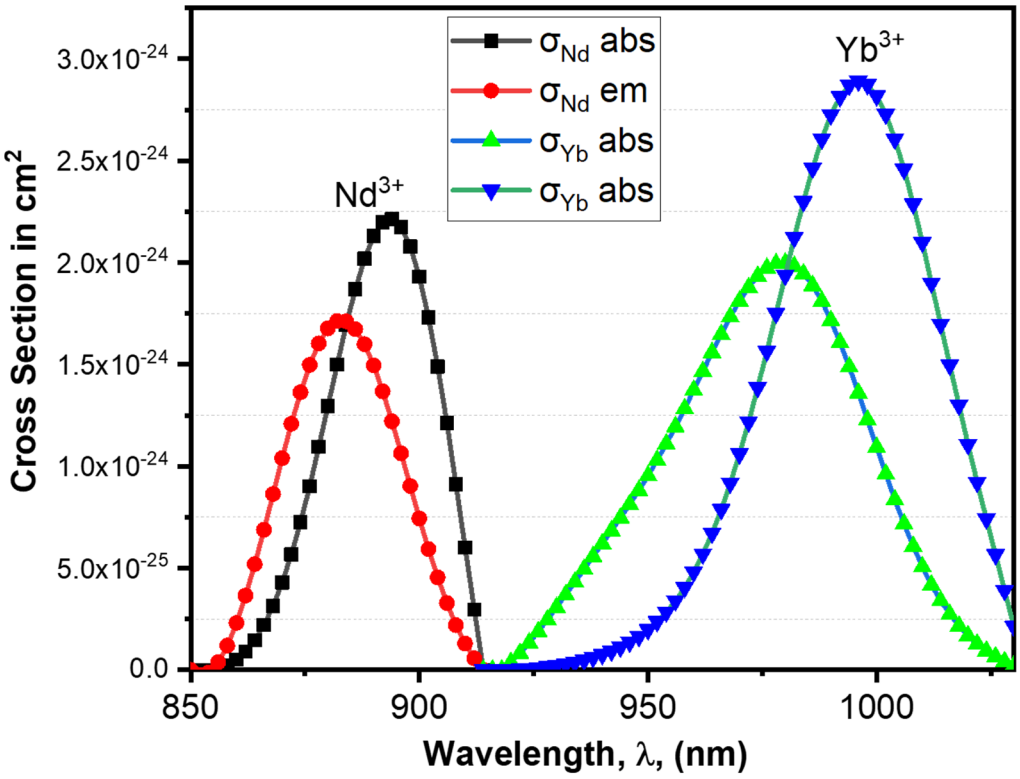

Figure 6. Absorption and emission cross section of prepared glass PZLBNdYb.

Figure 7a,b shows the measured MAC and LAC at 59.5, 622, 1170 and 1330 keV. The recorded values of MAC and LAC for the proposed sample at 662 keV were 0.081 ± 0.03 and 0.225 ± 0.13 in cm^2/g, respectively. These values were better than commercially available glass shielding materials, such as RS253 and G18 [39]. The measured half-value layer, HVL; and mean free path, MFP; at the same specific energies 59.5, 622, 1170 and 1330 keV were obtained; Figure 7c,d. The values for HVL and MFP of the present glass at 662 keV were 2.20 ± 0.82 and 3.17 ± 1.18 cm, respectively.

The HVL signifies the material thickness that reduces the intensity of radiation to half. HVLs are reported for commercial materials, such as windows glass (4.73 cm), serpentine (4.07 cm), concrete (3.87 cm), SCHOOT glass RS253 (3.65 cm), hematite serpentine (3.6 cm), Ilmenite (2.63 cm) and SCHOOT glass RS323 (2.48 cm) [40,41]. Thus, our glass had a lower HVL, which is better than commercial material. It was correlated with codoped heavy compounds of Nd^{3+}/Yb^{3+} ions in its structure of the host glass $40P_2O_5$-30ZnO-20LiCl-$10BaF_2$ to increase interaction probability, and more electrons are effectively available at low energy levels.

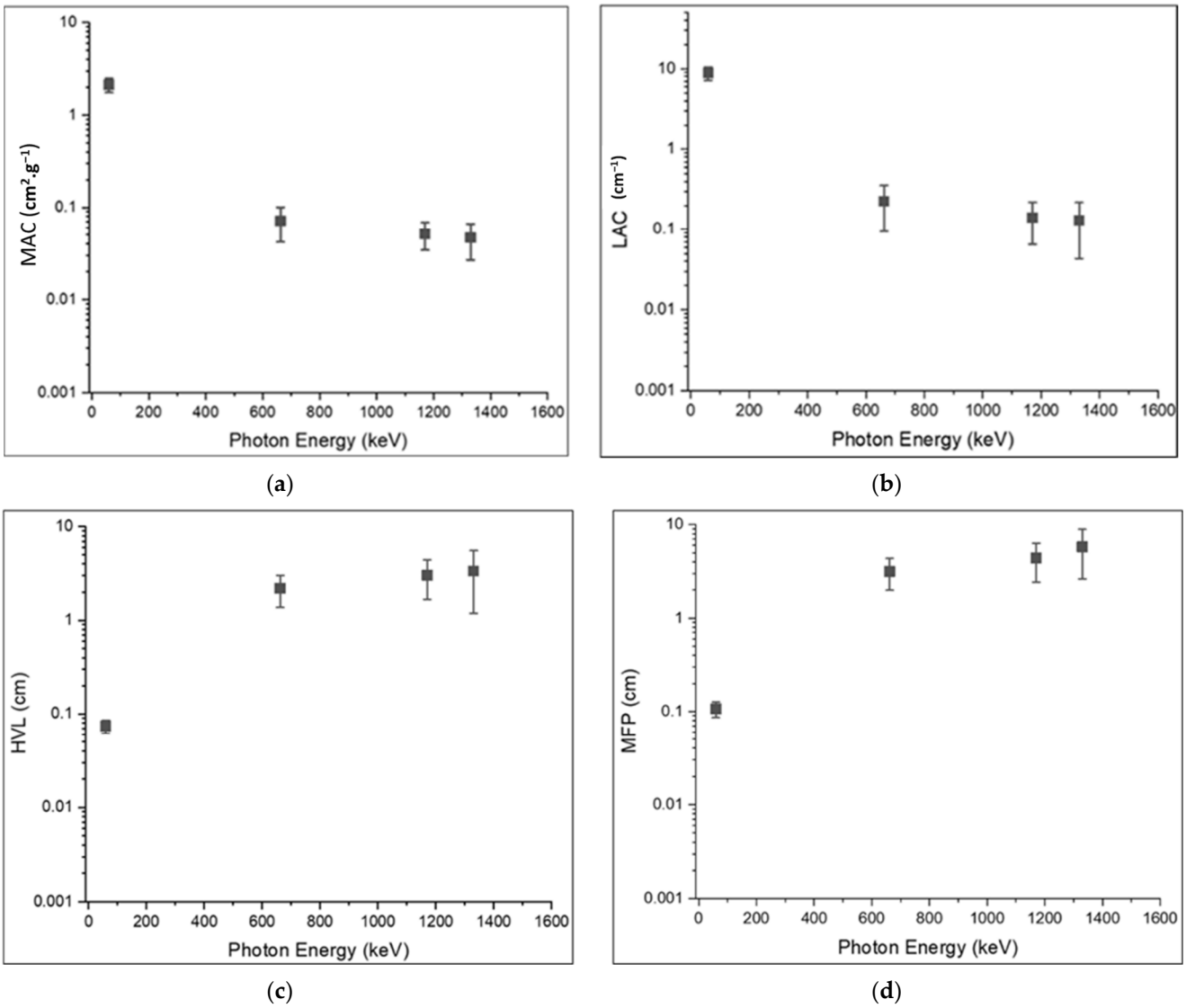

Figure 7. The measured and theoretical shielding parameters for TeTaNbZn glass samples at 59.5, 622, 1170 and 1330 keV: (**a**) MAC; (**b**) LAC; (**c**) HVL; and (**d**) MFP.

4. Conclusions

The incorporated double ions of Nd^{3+}/Yb^{3+} into $40P_2O_5$-30ZnO-20LiCl-$10BaF_2$ glass increase the optical energy gap (4.41eV), which is a suitable active medium for laser glasses. We found that the JO intensity parameters of the produced glass follow the trend $\Omega_6 > \Omega_4 > \Omega_2$, which has a high spectroscopic quality factor (Ω_4/Ω_6) equal to 0.84. This is larger than standard laser host Nd^{3+}:YAG.

The fabricated glass had a large value of $\sigma_{em}(\lambda)$, 2.23×10^{-24} cm^2, with the corresponding transition level Nd^{3+}: $^4F_{3/2} \rightarrow {}^4I_{9/2}$ and was 2.88×10^{-24} cm^2, attributable to Yb^{3+}:$^2F_{5/2} \rightarrow {}^2F_{7/2}$. Moreover, the gamma spectroscopic properties of the present glass showed a low half-value layer, which increases the interaction probability and creates more effective electrons at low energy. We conclude that the investigated glass has unique luminescence/gamma spectroscopic properties; hence, it can be used in photodynamic therapy surgery as a laser material in radiology rooms.

Author Contributions: B.C., conceptualization, methodology, investigation, writing—original draft and writing—review and editing; K.D., conceptualization, methodology, formal analysis, investigation and writing—original draft; M.S.A., methodology, writing—review and editing, investigation and visualization; K.I.H., formal analysis, investigation, visualization, writing—review and editing;

A.M.A., formal analysis, writing—original draft and visualization; N.E., methodology, investigation, writing—original draft and visualization; A.L.A., methodology, writing—original draft and visualization; K.F.A., methodology, writing—original draft and visualization; M.R., methodology, formal analysis, writing—review and editing and visualization; E.S.Y., conceptualization, methodology, investigation, funding acquisition, writing—review and editing and visualization. All authors have read and agreed to the published version of the manuscript.

Funding: This research was funded by the Deputyship for Research and Innovation, Ministry of Education in Saudi Arabia, for funding this research work through the project number IFP-KKU-2020/7.

Institutional Review Board Statement: Not applicable.

Informed Consent Statement: Not applicable.

Data Availability Statement: Not applicable.

Acknowledgments: The authors extend their appreciation to the Deputyship for Research and Innovation, Ministry of Education, Saudi Arabia, for funding this research work through project number IFP-KKU-2020/7. The authors thank Ramzi Maâlej for review and scientific editing the manuscript.

Conflicts of Interest: The authors declare no conflict of interest.

References

1. Dorosz, D.; Żmojda, J.; Kochanowicz, M.; Dorosz, J. Nd^{3+}/Yb^{3+} Doped Phosphate and Antimony Glasses for Optical Fibre Source. *Acta Phys. Pol. A* **2010**, *118*, 1108. [CrossRef]
2. Afef, B.; Alqahtani, M.M.; Hegazy, H.H.; Yousef, E.; Damak, K.; Maâlej, R. Green and near-infrared emission of Er^{3+} doped PZS and PZC glasses. *J. Lumin.* **2018**, *194*, 706–712. [CrossRef]
3. Lachheb, R.; Damak, K.; Assadi, A.A.; Herrmann, A.; Yousef, E.; Rüssel, C.; Maâlej, R. Characterization of Tm^{3+} doped TNZL glass laser material. *J. Lumin.* **2015**, *161*, 281–287. [CrossRef]
4. Damak, K.; Yousef, E.; AlFaify, S.; Rüssel, C.; Maâlej, R. Raman, green and infrared emission cross-sections of Er^{3+} doped TZPPN tellurite glass. *Opt. Mater. Express* **2014**, *4*, 597–612. [CrossRef]
5. Deguil, N.; Mottay, E.; Salin, F.; Legros, P.; Choquet, D. Novel diode-pumped infrared tunable laser system for multi-photon microscopy. *Microsc. Res. Technol.* **2004**, *63*, 23. [CrossRef]
6. Singh, V.P.; Badiger, N.M.; Kaewkhao, J. Radiation shielding competence of silicate and borate heavy metal oxide glasses: Comparative study. *J. Non-Cryst. Solids* **2014**, *404*, 167–173. [CrossRef]
7. Singh, K.; Singh, S.; Dhaliwal, A.S.; Singh, G. Gamma radiation shielding analysis of lead-flyash concretes. *Appl. Radiat. Isot.* **2015**, *95*, 174–179. [CrossRef]
8. Tijani, S.A.; Kamal, S.M.; Al-Hadeethi, Y.; Arib, M.; Hussein, M.A.; Wageh, S.; Dim, L.A. Radiation shielding properties of transparent erbium zinc tellurite glass system determined at medical diagnostic energies. *J. Alloy. Compd.* **2018**, *741*, 293–299. [CrossRef]
9. Qi, F.; Huang, F.; Wang, T.; Ye, R.; Lei, R.; Tian, Y.; Zhang, J.; Zhang, L.; Xu, S. Highly Er^{3+} doped fluorotellurite glass for 1.5 μm broadband amplification and 2.7 μm microchip laser applications. *J. Lumin.* **2018**, *202*, 132–135. [CrossRef]
10. Hussein, K.I.; Alqahtani, M.S.; Alzahrani, K.J.; Alqahtani, F.F.; Zahran, H.Y.; Alshehri, A.M.; Yahia, I.S.; Reben, M.; Yousef, E.S. The Effect of ZnO, MgO, TiO_2, and Na_2O Modifiers on the Physical, Optical, and Radiation Shielding Properties of a TeTaNb Glass System. *Materials* **2022**, *15*, 1844. [CrossRef]
11. Lalla, E.A.; Konstantinidis, M.; De Souza, I.; Daly, M.G.; Martín, I.R.; Lavín, V.; Rodríguez-Mendoza, U.R. Judd-Ofelt parameters of RE^{3+}-doped fluorotellurite glass (RE^{3+} = Pr^{3+}, Nd^{3+}, Sm^{3+}, Tb^{3+}, Dy^{3+}, Ho^{3+}, Er^{3+}, and Tm^{3+}). *J. Alloys Compd.* **2020**, *845*, 156028. [CrossRef]
12. Judd, B.R. Optical absorption intensities of rare-earth ions. *Phys. Rev.* **1962**, *127*, 750–761. [CrossRef]
13. Ofelt, G.S. Intensities of crystal spectra of rare−earth ions. *J. Chem. Phys.* **1962**, *37*, 511–520. [CrossRef]
14. Zaman, F.; Srisittipokakun, N.; Rooh, G.; Khattak, S.A.; Singkiburin, N.; Kim, H.J.; Sangwaranatee, N.; Kaewkhao, J. Investigation of Li_2O–Gd_2O_3–MO–B_2O_3–Nd_2O_3 (MO=Ba/Bi) glasses for laser applications by Judd–Oflet (J–O) theory. *J. Lumin.* **2019**, *215*, 116639. [CrossRef]
15. Afef, B.; Hegazy, H.H.; Algarni, H.; Yang, Y.; Damak, K.; Yousef, E.; Maâlej, R. Spectroscopic analysis of trivalent Nd^{3+}/Yb^{3+} ions codoped in PZS host glasses as a new laser material at 1.06 μm. *J. Rare Earths* **2017**, *35*, 361–367. [CrossRef]
16. James, J.T.; Jose, J.K.; Manjunatha, M.; Suresh, K.; Madhu, A. Structural, luminescence and NMR studies on Nd^{3+}-doped sodium–calcium-borate glasses for lasing applications. *Ceram. Int.* **2020**, *46*, 27099–27109. [CrossRef]
17. Yusof, N.N.; Ghoshal, S.K.; Jupri, S.A. Luminescence of Neodymium Ion-Activated Magnesium Zinc Sulfophosphate Glass: Role of Titanium Nanoparticles Sensitization. *Opt. Mater.* **2020**, *109*, 110390. [CrossRef]
18. Siva Rama Krishna Reddy, K.; Swapna, K.; Mahamuda, S.; Venkateswarulu, M.; Rao, A.S. Structural, optical and photoluminescence properties of alkaline-earth boro tellurite glasses doped with trivalent Neodymium for 1.06 μm optoelectronic devices. *Opt. Mater.* **2021**, *111*, 110615. [CrossRef]

19. Elbashar, Y.H.; Rayan, D.A. Judd Ofelt Study of Absorption Spectrum for Neodymium Doped Borate Glass. *Int. J. Appl. Chem.* **2016**, *12*, 59–66.
20. De Sa, G.F.; Malta, O.L.; de Mello Donegá, C.; Simas, A.M.; Longo, R.L.; Santa-Cruz, P.A.; da Silva, E.F., Jr. Spectroscopic properties and design of highly luminescent lanthanide coordination complexes. *Coord. Chem. Rev.* **2000**, *196*, 165–195. [CrossRef]
21. Carnall, W.T.; Hessler, J.P.; Wagner, F., Jr. Transition probabilities in the absorption and fluorescence spectra of lanthanides in molten lithium nitrate-potassium nitrate eutectic. *J. Phys. Chem.* **1978**, *82*, 2152. [CrossRef]
22. Singh, G.; Tiwari, V.S.; Gupta, P.K. Spectroscopic analysis on the basis Judd–Ofelt theory of Nd^{3+} in $(Y_{0.985}Nd_{0.015})_2O_3$: A transparent laser-host ceramic. *Mater. Res. Bull.* **2014**, *60*, 838–842. [CrossRef]
23. Kaminskii, A.A. *Laser Crystals: Their Physics and Properties*; Springer: Berlin, Germany, 1981; pp. 157–158.
24. Krupke, W.F. Induced-emission cross sections in neodymium laser glasses. *IEEE J. Quant. Electron.* **1971**, *7*, 153. [CrossRef]
25. Campbell, J.H.; Suratwala, T.I.; Suratwala, T.I. Continuous melting of phosphate laser glasses. *J. Non-Cryst. Solids* **2000**, *263–264*, 342–357. [CrossRef]
26. Jayasankar, C.K.; Balakrishnaiah, R.; Venkatramu, V.; Joshi, A.S.; Speghini, A.; Bettinelli, M. Luminescence characteristics of Nd^{3+}-doped K-Ba-Al-fluorophosphate laser glasses. *J. Alloy Comp.* **2008**, *451*, 697–701. [CrossRef]
27. Gupta, G.; Sontakke, A.D.; Karmakar, P.; Biswas, K.; Balaji, S.; Saha, R.; Sen, R.; Annapurna, K. Influence of bismuth on structural, elastic and spectroscopic properties of Nd^{3+} doped zinc–boro-bismuthate glasses. *J. Lumin.* **2014**, *149*, 163–169. [CrossRef]
28. Binnemans, K.; Van Deun, R.; Gorller-Walrand, C.; Adam, J.L. Spectroscopic properties of trivalent lanthanide ions in fuorophosphate glasses. *J. Non-Cryst. Solids* **1998**, *238*, 11–29. [CrossRef]
29. Shoaib, M.; Rooh, G.; Chanthima, N.; Kim, H.J.; Kaewkhao, J. Luminescence properties of Nd^{3+} ions doped P_2O_5-Li_2O_3-GdF_3 glasses for laser applications. *Opt.-Int. J. Light Electron. Opt.* **2019**, *199*, 163218. [CrossRef]
30. Prasad, V.R.; Dhamodaraiah, S.; Babu, S.; Ratnakaram, Y.C. Spectroscopic investigation of Nd^{3+} doped zinc phosphate glasses for NIR emission at 1.05 μ-m. *Mater Today Proc.* **2016**, *3*, 3805–3809. [CrossRef]
31. Jorgensen, C.K.; Reisfeld, R. Judd-Ofelt parameters and chemical bonding. *J. Common Met.* **1983**, *93*, 107–112. [CrossRef]
32. Reisfeld, R. Luminescence and prediction of transition probabilities for solar energy and lasers. *J. Common. Met.* **1985**, *112*, 9–18. [CrossRef]
33. Jacobs, R.; Weber, M. Dependence of the $^4F_{3/2} \rightarrow {}^4I_{11/2}$ induced-emission cross section for Nd^{3+} on glass composition. *IEEE J. Quant. Electron.* **1976**, *12*, 102–111. [CrossRef]
34. Riseberg, L.A.; Weber, M.J. Relaxation phenomena in rare-earth luminescence. *Prog. Opt.* **1977**, *31*, 89–159.
35. Fares, H.; Jlassi, I.; Hraiech, S.; Elhouichet, H.; Ferid, M. Radiative parameters of Nd^{3+}-doped titanium and tungsten modified tellurite glasses for 1.06 μm laser materials. *J. Quant. Spectrosc. Radiat. Transf.* **2014**, *147*, 224–232. [CrossRef]
36. Manasa, P.; Srihari, T.; Basavapoornima, C.; Joshi, A.S.; Jayasankara, C.K. Spectroscopic investigations of Nd^{3+} ions in niobium phosphate glasses for laser applications. *J. Lumin.* **2019**, *211*, 233–242. [CrossRef]
37. Prasad, R.N.A.; Praveena, R.; Vijaya, N.; Babu, P.; Krishna Mohan, N. Neodymiumdoped magnesium phosphate glasses for NIR laser applications at 1.05 μm. *Mater. Res. Express* **2019**, *6*, 096204.
38. Ramteke, D.D.; Kroon, R.E.; Swart, H.C. Infrared emission spectroscopy and upconversion of ZnO-Li_2O-Na_2O-P_2O_5 glasses doped with Nd^{3+} ions. *J. Non-Cryst. Solids* **2017**, *457*, 157–163. [CrossRef]
39. Chanthima, N.; Kaewkhao, J. Investigation of radiation shielding parameters of bismuth borosilicate glass from 1 keV to 100 GeV. *Ann. Nucl. Energy* **2013**, *55*, 23–28. [CrossRef]
40. Chanthima, N.; Kaewkhao, J.; Limkitjaroenporn, P.; Tuscharoen, S.; Kothan, S.; Tungjai, M.; Kaewjaeng, S.; Sarachai, S.; Limsuwan, P. Development of BaO–ZnO–B_2O_3 glasses as a radiation shielding material. *Radiat. Phys. Chem.* **2017**, *137*, 72–77. [CrossRef]
41. Cheewasukhanont, W.; Limkitjaroenporn, P.; Sayyed, M.I.; Kothan, S.; Kim, H.J.; Kaewkhao, J. High density of tungsten gadolinium borate glasses for radiation shielding material: Effect of WO_3 concentration. *Radiat. Phys. Chem.* **2022**, *192*, 109926. [CrossRef]